Dynamics Modelling and Adaptive Identification: Towards Improved Human-Robot Interaction in Collaborative Systems

Saixuan Chen[1,*], Kaiye Zhou[1], Xiaolong Zhang[1] and Zina Zhu[1]

[1]*Shanghai University of Engineering Science, 333 Longteng Road, Songjiang District, Shanghai 201620, China*

Abstract: This article presents a novel approach to enhancing human-robot collaboration and safety through advanced dynamic modelling and adaptive identification techniques. We introduce a comprehensive methodology that integrates motion trajectory design with real-time torque detection, addressing the critical limitations of conventional systems that rely on costly joint torque sensors. By simultaneously identifying friction forces in an integrated joint and a simplified two-bar mechanism, our approach leverages existing kinematic and dynamic models to achieve precise dynamic parameter identification. The proposed method significantly advances the fields of drag-teaching and collision detection by eliminating the need for force sensors, thus making it more feasible for mass-produced robotic systems. Our findings demonstrate that accurate dynamic modelling is essential for effective zero-force control, particularly in high-speed drag-teaching scenarios, where inertia and friction present substantial challenges. Experimental validation confirms the efficacy of our dynamic feed-forward controller design and the adaptability of drag-teaching parameters, leading to improved operational flexibility and safety in collaborative environments. This research contributes a critical framework for future developments in intelligent robotic systems, providing a robust basis for integrating advanced human-robot interactions in industrial applications.

Keywords: Six degrees of freedom manipulator, Parameter identification, Feed-forward control, Drag-teaching, Dynamic modelling.

1. INTRODUCTION

With the implementation and promotion of 'smart manufacturing' across various industries, collaborative robots play an essential role in realizing this production process. Among these, human-machine integration is a crucial development direction for intelligent robots. Compared to traditional robots, human-machine collaborative robots offer advantages such as flexible operation, strong environmental adaptability, and the ability to facilitate natural human-machine interaction. Figure **1** illustrates a lightweight collaborative robot equipped with six integrated joints capable of achieving translation and rotation across six degrees of freedom at its end effector. Additionally, various tools can be attached to the robot's end effector to accommodate different working conditions.

For collaborative robots, human-robot collaboration is essential for the in-depth application of intelligent robots; thus, improving collaboration and safety is a critical issue for practical implementation. This encompasses two key functions of intelligent robots: drag teaching and collision detection [1]. Drag teaching allows the robot to be freely dragged and to reproduce the drag trajectory by applying external forces, thereby simplifying the robot's operation process. Conversely, collision detection enables the robot to accurately perceive external obstacles and respond accordingly, thus preventing harm to humans in the same environment.

*Address correspondence to this author at the Shanghai University of Engineering Science, 333 Longteng Road, Songjiang District, Shanghai 201620, China; E-mail: chensx499796981@126.com

Numerous theoretical studies have addressed the realization of two key functions: drag teaching and collision detection. However, most studies rely on joint torque sensors or six-dimensional force sensors. Although these methods effectively detect collision forces and predict the driving torque of individual joints, high-precision sensors are expensive, complicating their direct application to mass-produced robots. The most common method for achieving drag teaching and collision detection without force sensors is the zero-force control method. This control method enables the robot to move in response to external forces, thus minimizing the effects of friction and gravity during operation. Currently, the most widely used zero-force control methods primarily rely on compensating for gravity and friction [2, 3]. However, during actual operation, the increased speed of drag teaching raises the inertia effects of each joint, leading to a deterioration in flexibility. Therefore, the key to zero-force control lies in compensating for gravitational and frictional moments, which requires an accurate dynamic model of the robot; otherwise, accuracy and real-time performance cannot be ensured.

Dynamic modelling is a crucial topic in robotics. Developing an accurate dynamic model is essential for force analysis, trajectory planning, and control of multi-degree-of-freedom manipulators. However, multi-degree-of-freedom manipulators possess numerous dynamic parameters, with strong coupling between joints, complicating the identification of the actual dynamic model.

In recent years, several methods have been proposed both domestically and internationally,

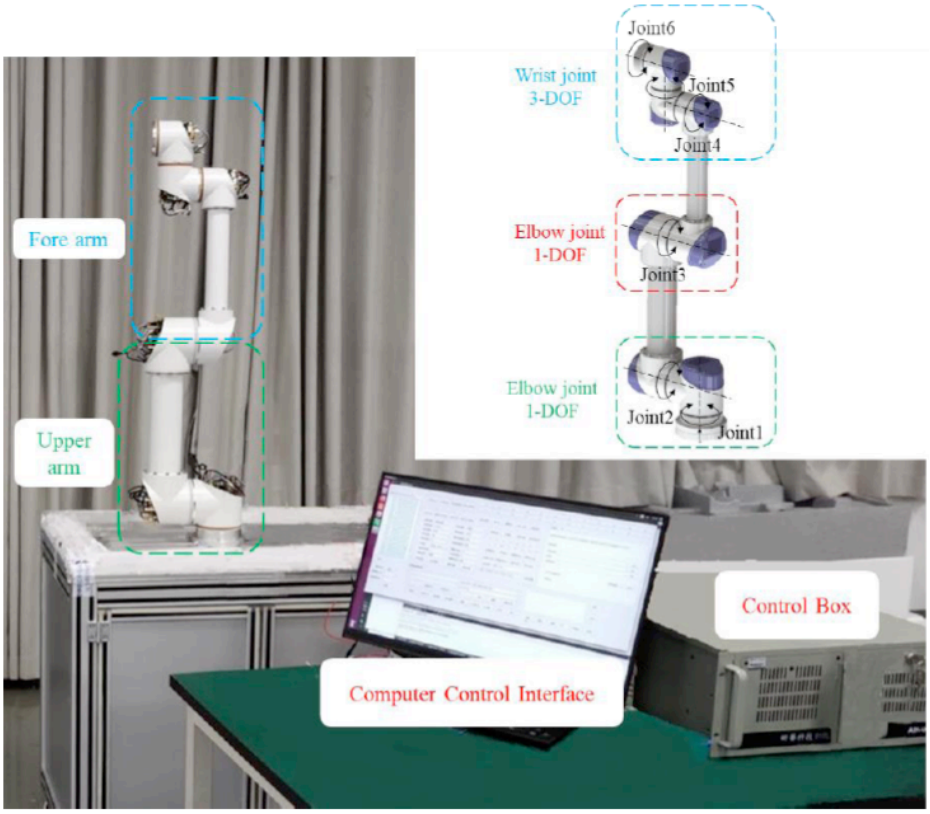

Figure 1: Six-axis lightweight collaborative robot.

including disassembly measurement, CAD methods, theoretical identification, one-time identification, and overall identification to determine the parameters of the robot's dynamic model [4-9]. In the disassembly measurement method, Armstrong *et al*. dismantled the PUMA560 robot and used specialized instruments to measure each joint individually, obtaining relevant inertial parameters [10-12]. Although the single-joint inertial parameters obtained through this method are highly accurate, the measurement conditions are stringent, the process is cumbersome, and the influence of joint coupling cannot be avoided. CAD methods, such as the one proposed by Wu Zhiyun, are based on finite element analysis; however, accurate dynamic models cannot be identified due to issues like assembly errors [13]. The one-shot identification method [14] proposed by Zhang Shiyuan *et al*. separates the front and rear three joints into two sections, establishes excitation trajectory signals for each, and conducts a single identification of the dynamic parameters. This method, based on least squares expansion, effectively eliminates experimental errors from multiple identifications and enhances calculation accuracy. However, this method does not yield single-joint identification parameters and can only be used for overall analysis. T The theoretical identification method relies on an accurate dynamic model.

So far, the proposed theoretical modelling methods are relatively mature, including the Newton–Euler method, the Lagrange method, the virtual work principle, the rotational algebra method, and the Kane method [15, 16]. The dynamic model often deviates significantly from the robot's actual dynamic behaviour, making direct application challenging. This challenge can be attributed to three factors: (1) the kinetic parameters of the three-dimensional robot model, such as rod mass and inertia, are often inaccurate; (2) the additional driving torque generated by joints due to gap collisions and friction during actual operation is difficult to model accurately; and (3) for robots with integrated joints, the torque sensitivity coefficient of the motor is often unstable and must be identified during actual use.

Based on the joint driving torque components obtained through theoretical modelling and experimental data identification, this paper proposes a synchronous identification method for the torque sensitivity coefficient and joint friction force in integrated joints. The proposed method, based on the theoretical gravity torque model, can simultaneously obtain multiple identification parameters. Finally, a six-degree-of-freedom robot is employed as the research subject to validate the accuracy and feasibility of the proposed dynamic parameter identification method.

2. DYNAMICAL PARAMETER IDENTIFICATION METHOD

2.1. Theoretical Modelling of Robot Dynamics

Zero-moment control technology is essential for enabling robots to perform functions such as collision detection and drag teaching. The connection between the motor and the load can be modelled as a torsional spring, which represents the flexibility of the joint, as shown in Formula 1. The dynamic model can be expressed as follows.

$$\tau_m = B\ddot{\theta} + M(q)\ddot{q} + C(q,\dot{q})\dot{q} + G(q) + \tau_f \quad (1)$$

τ_m is the output torque of the motor. K_m is the motor torque constant, B is the rotational inertia, $G(q)$ represents the gravitational moment, τ_f is the friction force, and q is the rotational angle.

2.2. Robot Single Joint Identification Experiment

The single-axis dynamic model identification of each joint is conducted based on the robot body. The primary method involves keeping other joints stationary while moving the target joint under various robot poses and operating speeds. During the experiment, the joint's position, angular velocity, angular acceleration, and driving current are recorded. This data is then combined with the established robot dynamics model to identify the motor torque sensitivity coefficient, basic dynamic parameters, and friction model of the robot joint.

2.3. Verification Experiment of Multi-Axis Comprehensive Trajectory Motion

Based on the actual dynamic model obtained for each joint, we designed the motion trajectory for the robot to operate simultaneously across multiple axes. Next, we collected the position, angular velocity, angular acceleration, and driving current data for each joint during operation. We then substituted this data into the identified single-joint dynamic model to verify its accuracy.

2.4. Applied to the Actual Function of the Robot

Here, we applied the verified dynamic model of robot identification to the design of the drive-level dynamic feed-forward controller to compensate for the gravity and friction forces that occupy the dominant position in the driving moment, effectively improving the single-axis tracking accuracy. Concurrently, this model is used for parameter adjustment in drag teaching to evaluate its effectiveness. The primary indicator is the external force required for the smooth operation of the dragging robot, which eliminates the tedious trial-and-error process for parameter adjustment.

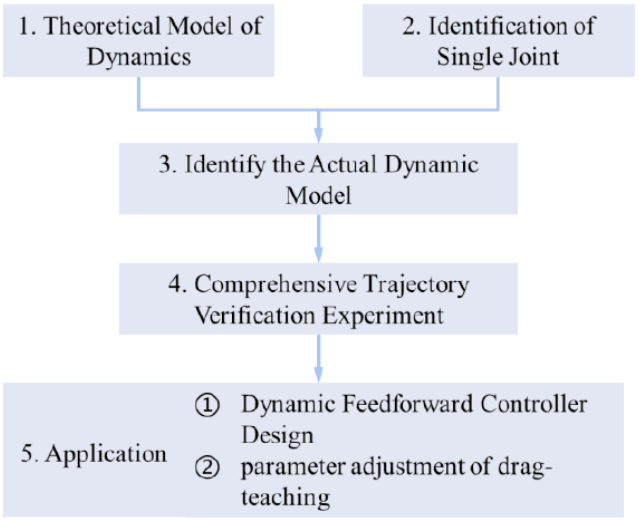

Figure 2: Research idea of this project.

3. EXPERIMENTS AND RESULT ANALYSIS

3.1. Robot Dynamics Model

The robot dynamics model established in previous research can be used directly after a simple verification of the correctness of its modelling process and results [17]. Therefore, the modelling process will not be repeated here. Among these, the analytical expression for the gravitational component in the driving torque of each joint is presented in Formula (2).

$$\begin{aligned}
G_1 &= 0 \\
G_2 &= -40.87\cos(q_2) - 18.64\cos(q_{23}) - 0.35\cos(q_{234})\sin(q_5) \\
&\quad + 1.69\cos(q_{23})\sin(q_4) + 1.69\sin(q_{23})\cos(q_4) \\
G_3 &= -18.64\cos(q_{23}) - 0.35\cos(q_{234})\sin(q_5) + 1.69\cos(q_{23})\sin(q_4) \\
&\quad + 1.69\sin(q_{23})\cos(q_4) \\
G_4 &= -0.35\cos(q_{234})\sin(q_5) + 1.69\cos(q_{23})\sin(q_4) + 1.69\sin(q_{23})\cos(q_4) \\
G_5 &= -0.35\cos(q_{234})\sin(q_5) \\
G_6 &= 0
\end{aligned} \quad (2)$$

In the formula, G_i represents the gravity component of the i-th joint (i=1,2,…6). The compensation value for the gravitational moment (G_i) to be overcome by each joint was calculated based on the gravitational moments of the six joints in various positions. The compensating torque of joint gravity can be calculated by using the dynamic equation. As shown in Formula (2), the gravity component of each joint is primarily expressed as a trigonometric function. Additionally, there is coupling between the joints, and their angles affect the gravity component. If the positions of the other joints are fixed and only one joint is operated, the gravity component of that joint will correspond to the trigonometric function of its position. In turn, this will be

used as the basis for performing the single-axis identification experiment.

3.2. Experiment and Analysis of Joint 1 Uniaxial Identification

Joint 1 is the motor located at the base of the robot, enabling the body to rotate around the vertical axis. Based on the operation mode of this joint, it can be inferred that the inertial force is negligible during the uniform motion stage, when its acceleration is relatively low. Additionally, the driving torque primarily serves to overcome friction, which may be influenced by the running speed and the robot's posture. To analyse the dynamic characteristics of Joint 1, the other joints are initially kept stationary, and the robot is then positioned vertically to initiate reciprocating motion within a specified range, followed by setting various speed levels. Subsequently, the driving current and joint motion data are collected to validate the relationship between driving torque and joint speed. Next, the robot's posture is adjusted to tilt while maintaining the same speed and range of motion during the reciprocating motion. Finally, data are collected again to validate the relationship between driving torque and robot posture. The two postures are illustrated in Figure **3**.

Next, to verify their relationship, we plot the velocity and current curves of Joint 1 for each experiment, as shown in Figures **4** through **9** below.

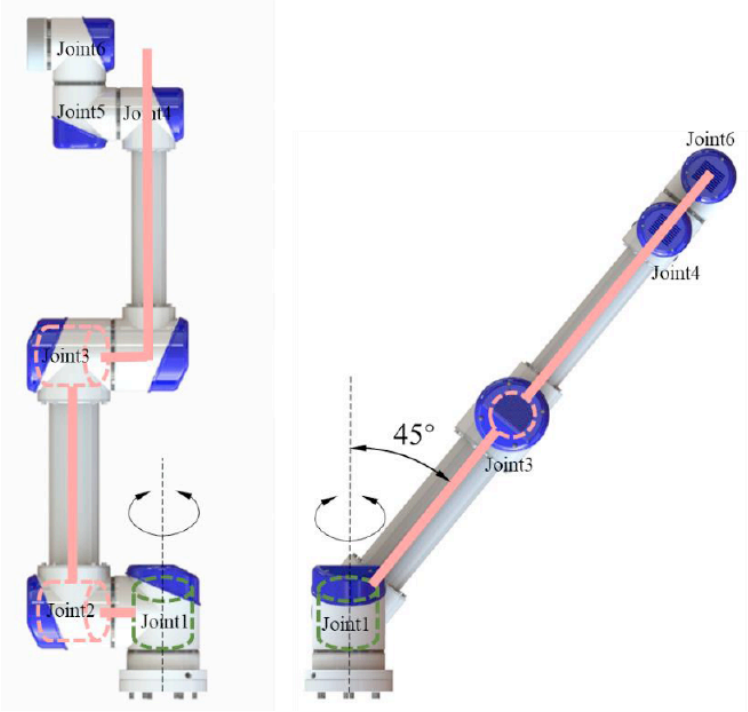

Figure 3: Two robot poses for joint 1 motion experiment.

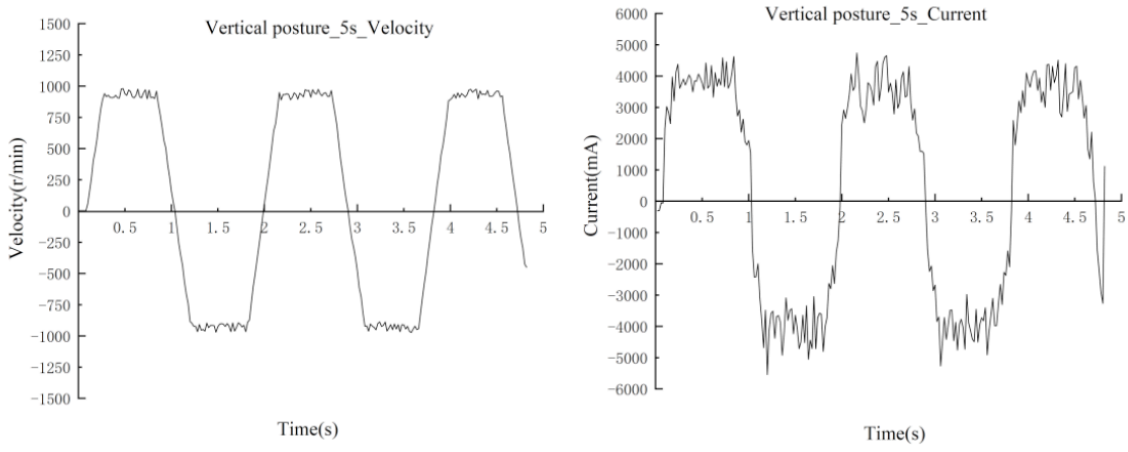

(**a**) joint velocity (**b**) joint current

Figure 4: Result curve of vertical posture experiment 1.

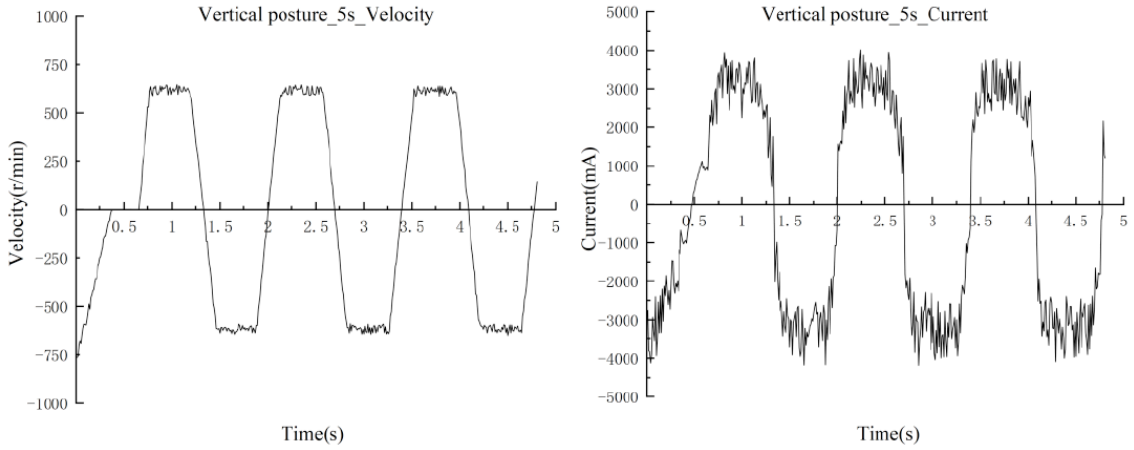

(**a**) joint velocity (**b**) joint current

Figure 5: Result curve of vertical posture experiment 2.

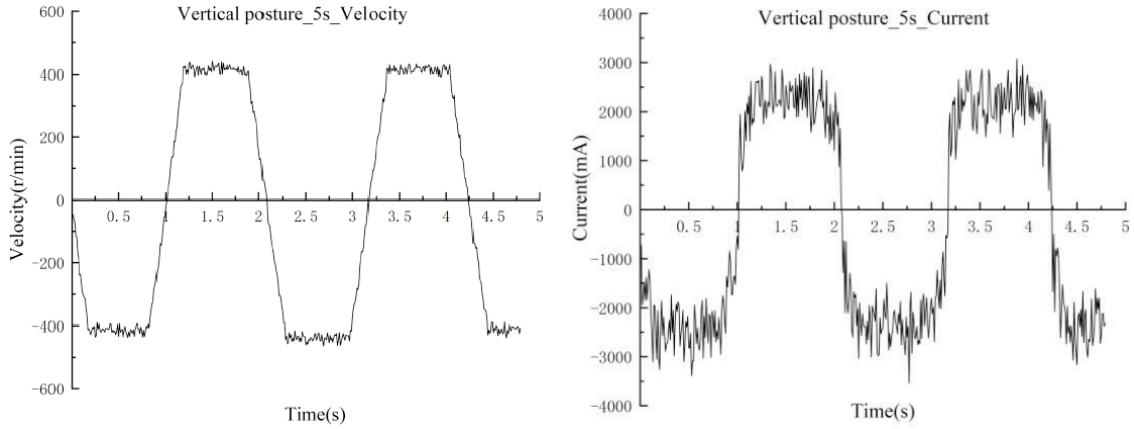

(**a**) joint velocity (**b**) joint current

Figure 6: Result curve of vertical posture experiment 3

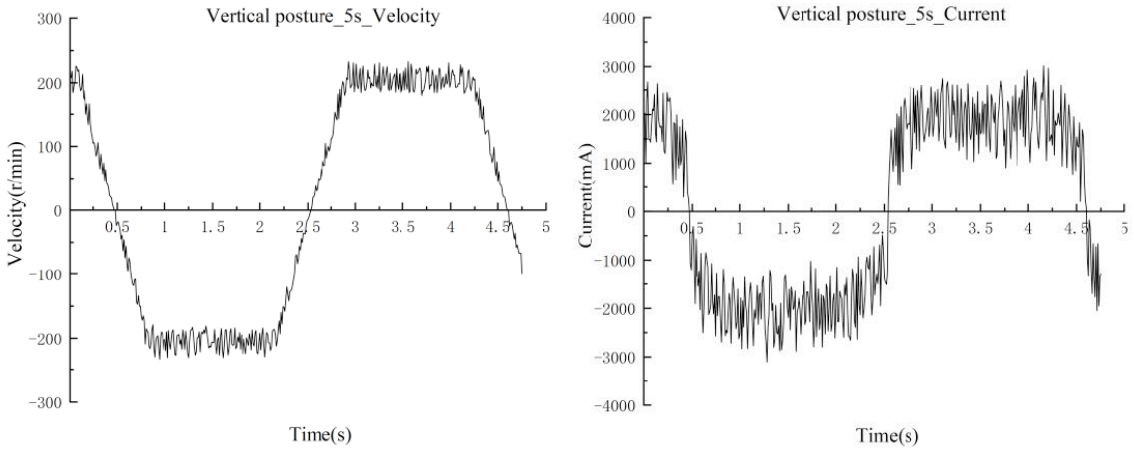

(**a**)-joint velocity (**b**)-joint current

Figure 7: Result curve of vertical posture experiment 4.

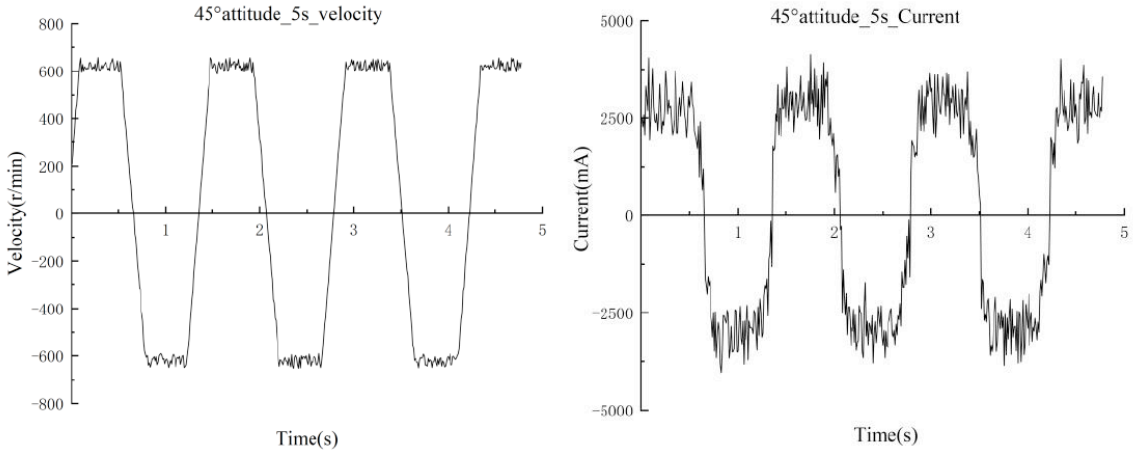

(**a**) joint velocity (**b**) joint current

Figure 8: Result curve of tilt posture experiment 1.

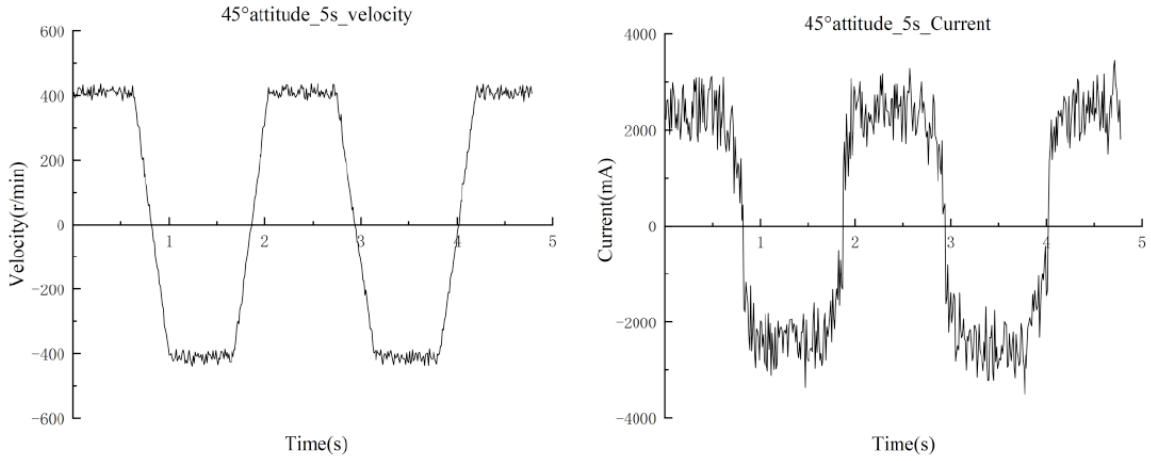

(**a**) joint velocity (**b**) joint current

Figure 9: Result curve of tilt posture experiment 2.

The above figures indicate a strong correlation between the driving current curve of Joint 1 and the velocity curve. Additionally, when the velocity varies, the peak value of the corresponding current curve also changes, indicating that the friction force of Joint 1 is a function of speed. Using the steady running speed from each experiment in the vertical posture as the abscissa and the absolute average value of the corresponding driving current as the ordinate, we plot the speed-current fitting curve, as shown in Figure **10**, and perform linear fitting to determine the correlation between them.

Concurrently, the two sets of experimental results for the tilted posture are included in the figure and represented by the orange dots in Figure **10**. As shown, under the same running velocity, the differences in driving current when the robot is vertical versus when it is inclined at 45° are 4.72% and 1.92%, respectively. This suggests that the influence of robot posture on the friction of Joint 1 can be considered negligible.

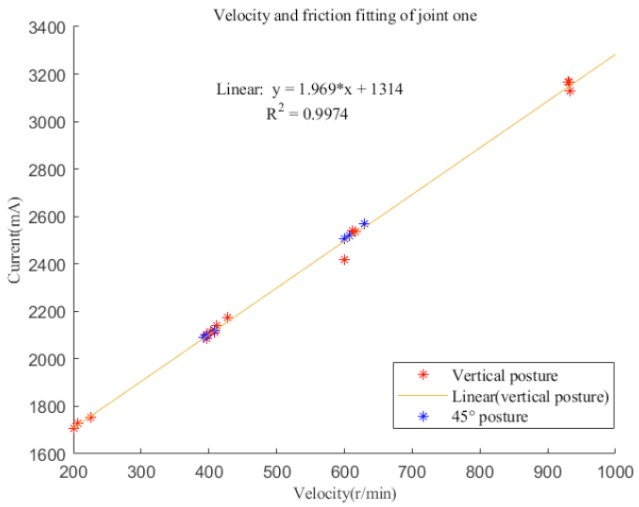

Figure 10: Fitting curve of joint 1 friction force identification experiment.

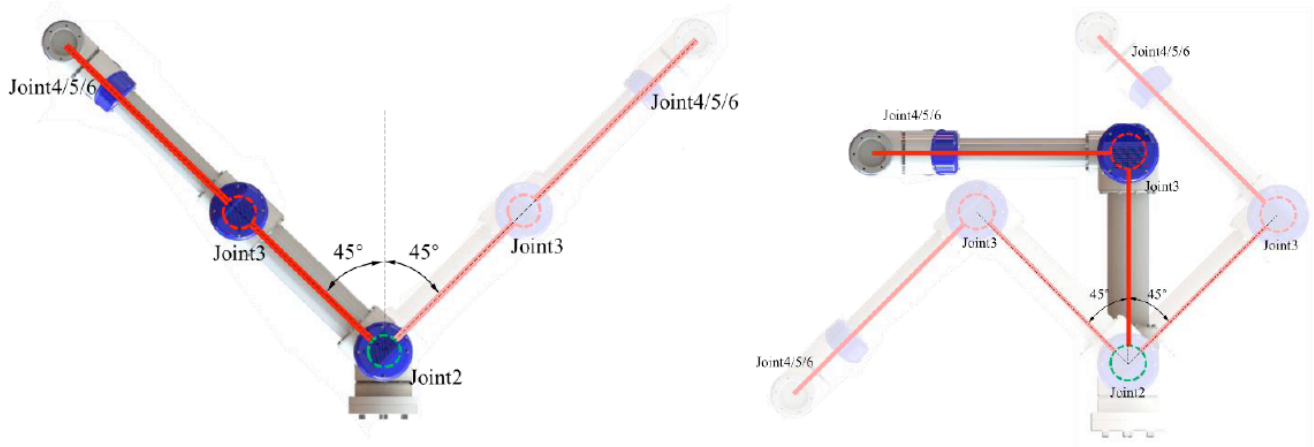

Figure 11: shows the joint 2 drive current curve obtained from the motion experiment in the vertical posture at five speed levels.

Meanwhile, the relationship between the driving current of Joint 1 and the motion speed, obtained through fitting, is expressed in Formula (3), where the unit of current is mA, the unit of velocity is $r/\min$, and the linear fitting correlation is 0.9974. The fitting results demonstrate a strong correlation.

$$I_1 = 2.0328v_1 + 1306.3\mathrm{sgn}(v_1) \tag{3}$$

Notably, among the seven groups of experiments included in the fitting, the three groups conducted at low speeds (100, 150, and 300 r/min) still exhibit a linear friction relationship, without clear static or Stribeck friction characteristics. In other words, the friction of the joint is higher when operating at low speeds close to stationary than when it is in motion. Therefore, the running velocity of the joint during drag teaching typically falls within this range, allowing for direct application of the fitting model.

3.3. Experiment and Analysis of Joint 2 Uniaxial Identification

The driving torque of Joint 2 includes gravity, inertial force, centrifugal force, Coriolis force, and friction. The inertial and centrifugal forces can be neglected due to the low speed and acceleration during drag teaching. Gravity is solely dependent on the robot's posture, and its model has been previously presented (Formula 3). The parameters of the gravity model are simulated using a SOLIDWORKS 3D model. In theory, the accuracy must be validated through experiments, which show that the friction force is related to the speed of this joint. This may be influenced by the gravitational load; therefore, it is essential to fit the friction force model through speed change and posture change experiments. Additionally, since the robot's integrated joints utilize custom motors, the torque sensitivity coefficients must also be identified. However, it is important to note that, according to Formula (4), the torque sensitivity coefficients and mechanism parameters are on opposite sides of the equation; thus, they cannot be identified simultaneously. Therefore, this study uses the mechanism parameters as the benchmark, assuming that the parameters obtained from 3D software and the gravity torque model derived from theoretical modelling are accurate.

$$\tau = K_t I \approx G(\theta) + f \tag{4}$$

The experimental design for the motion of Joint 2 is outlined as follows. First, the robot is maintained in a vertical posture while Joint 2 is reciprocated with uniform acceleration and deceleration within a range of ±45°. Various speed levels are then set to assess the influence of speed on the driving torque of Joint 2. Second, Joint 3 is bent by 90°, allowing the robot to repeat the previous motion in a right-angle posture, thereby enabling assessment of the impact of posture change on the driving torque of Joint 2. The two postures are illustrated in Figure **11**.

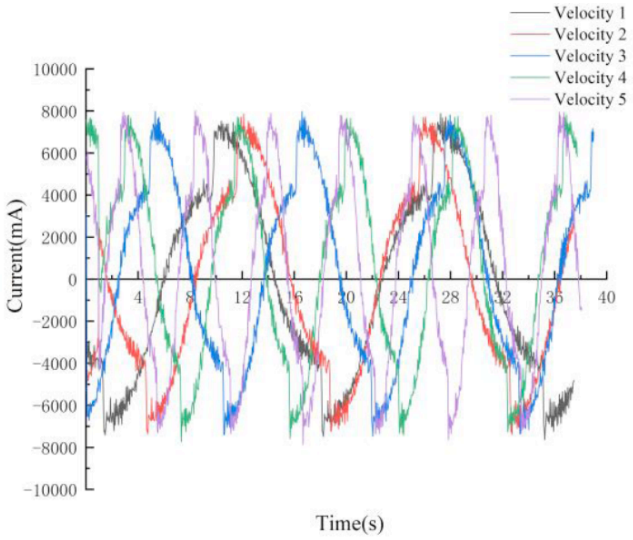

Figure 12: Current curves of joint 2 in vertical posture at five speed levels.

Figure **13** shows the joint 2 drive current curve obtained from the motion experiment in a right-angle posture at three speed levels.

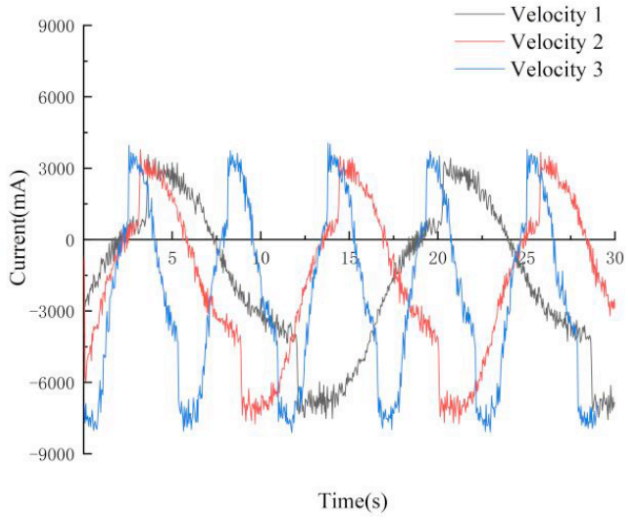

Figure 13: Current curves of joint 2 in right-angle posture at three speed levels.

As illustrated in Figures **12** and **13**, when the robot is in the same pose and only the joint motion speed is varied, the amplitudes of the resulting driving current curves remain largely consistent. This consistency is due to the identical experimental motion range for each group, resulting in uniform gravitational changes. This indicates that the amplitude of the driving torque is independent of the joint movement speed, suggesting that the viscous friction effect of Joint 2 is negligible. The experimental results for the two postures at the same speed are combined into a single figure, as illustrated in Figure **14**.

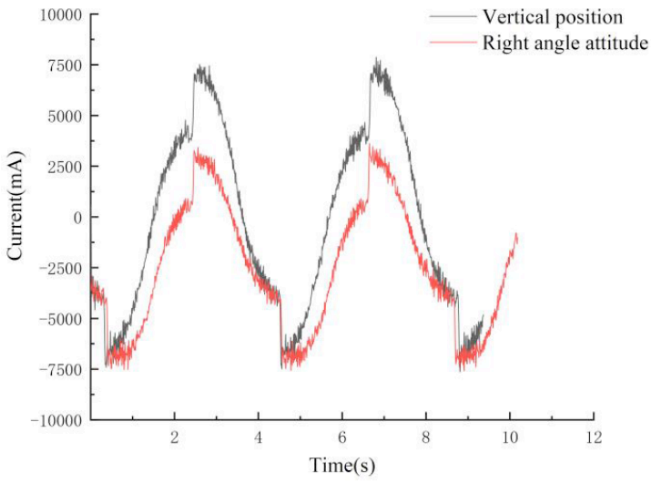

Figure 14: Comparison of current curves at the same speed and different postures.

As shown in Figure **14**, due to the specific nature of the two selected postures, the gravity torques at a certain motion limit position are identical, while they differ at the other limit position, validating the driving current curve. This characteristic indicates that the gravity torque is the primary component of the driving moment for Joint 2, and its trend dictates the overall trend of the driving moment.

Furthermore, to investigate the performance of the friction force in Joint 2, Figure **15** presents the drive current and joint rotation speed curves from the exercise test.

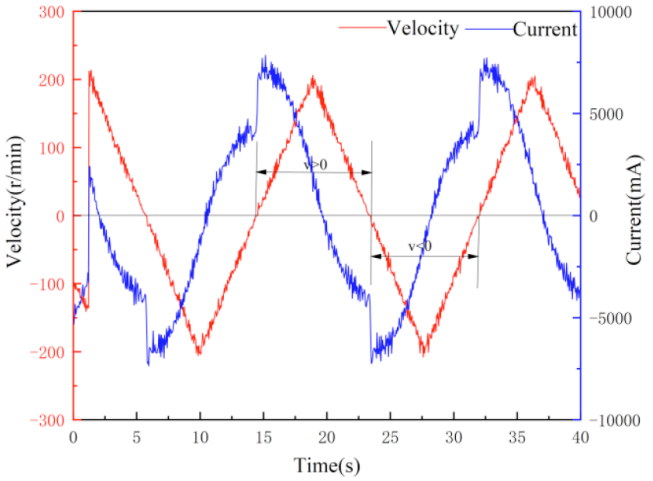

Figure 15: Current and speed results of exercise experiments.

As observed in Figure **15**, during this series of uniform acceleration and deceleration reciprocating motion experiments, the driving torque experiences a sudden change at the point of speed direction reversal. This abrupt change exhibits clear friction characteristics, indicating that the friction force opposes the object's movement. The sudden shift in driving torque when the speed direction changes reflect the alteration in the direction of the friction force. Moreover, the magnitude of this sudden change is equal to the sum of the absolute values of the forward and reverse friction forces.

Therefore, based on the theoretical gravity torque model and the identification experimental data, a synchronous identification scheme for the motor sensitivity coefficient and joint friction force is proposed. This scheme is detailed in Section 3.4. The actual dynamic model of Joint 2 obtained through this scheme is expressed as follows:

$$I_2 \approx \frac{G_2(\theta)}{K_{t2}} + \begin{cases} 1.759 & v > 0 \\ -1.526 & v < 0 \end{cases}, \tag{5}$$

Where $G_2(\theta)$ represents the calculated value of the gravity torque component for Joint 2, derived from the position information of the joints, and K_{t2}=7.1635 denotes the identified torque sensitivity coefficient of Joint 2.

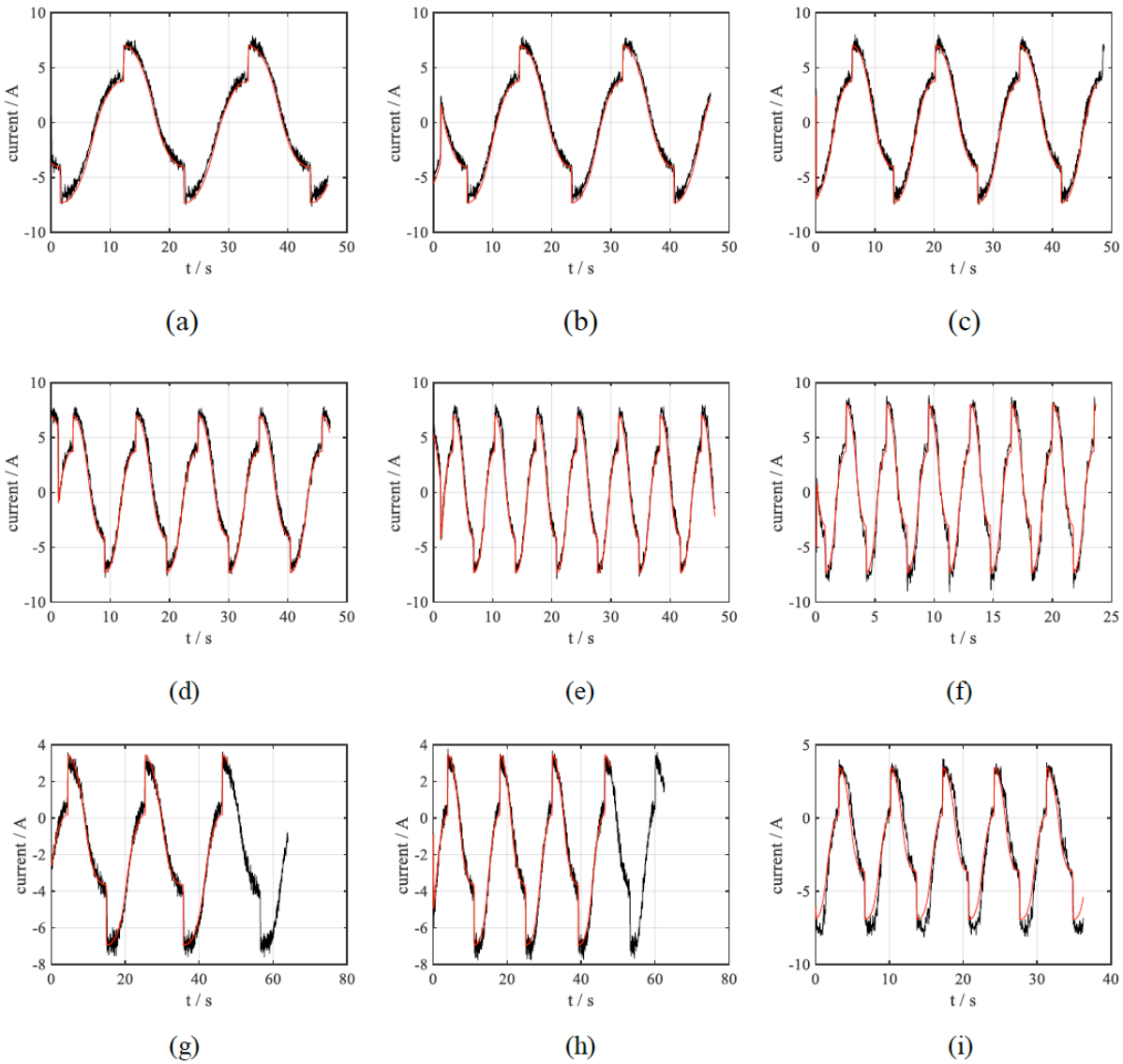

Figure 16: Verification results of joint 2 identification dynamic model.

The model is applied to other sets of experiments. As shown in Figure **16**, the black line represents the actual collected driving current curve, while the red line indicates the predicted current curve. The results demonstrate a good fit between the two curves.

3.4. Simultaneous Identification Scheme of Torque Sensitivity Coefficient and Joint Friction

Based on the joint driving torque components derived from theoretical modelling and the identification of experimental data, a synchronous identification scheme for the torque sensitivity coefficient and joint friction force in integrated joints can be proposed. This scheme, which uses gravity torque as a reference, allows for the simultaneous determination of both the motor's torque sensitivity coefficient and the numerical values of the joint's friction force during forward and reverse operation. The basic steps of the scheme are as follows:

(1) Based on the collected driving current and joint speed curves, the friction force is eliminated during changes in joint speed to obtain the actual current curve without joint friction force. Figure **17** serves as an example.

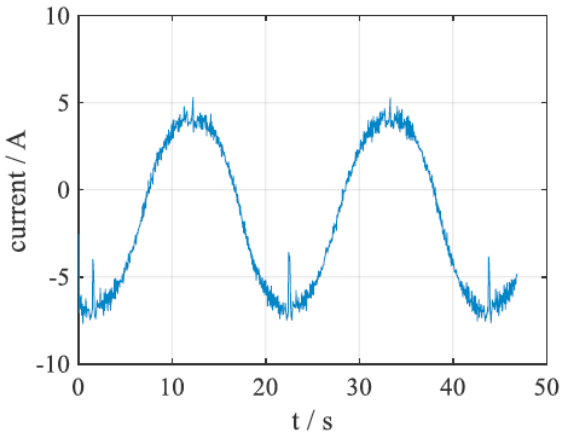

Figure 17: The driving current curve after eliminating the friction force of changing direction.

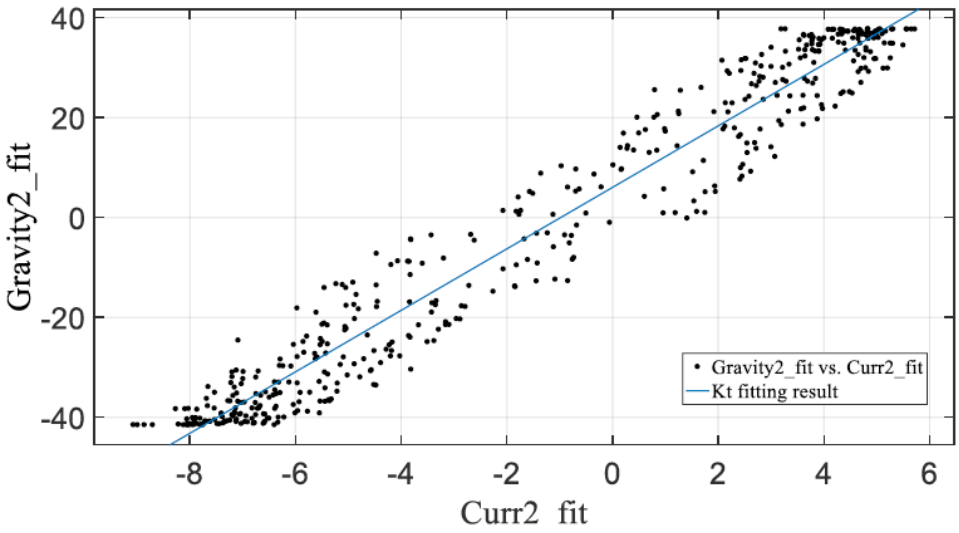

Figure 18: Fitting results of theoretical gravity torque and friction-less driving current.

(2) Using the collected joint position information, the gravity torque model from Equation (2) is applied to calculate the gravity component in the driving moment of the joint for this experiment. The resulting value is the theoretical numerical value.

(3) Using MATLAB's Curve Fitting Toolbox, the driving current curve is fitted after removing friction from the theoretical gravity torque curve. According to Equation (4), a linear relationship is expected between them, where the linear coefficient represents the torque sensitivity coefficient. It is important to note that since the friction force eliminated in step 1 is the sum of the forward and reverse friction forces, the linear intercept does not directly represent the friction force and requires further processing. Figure **18** displays the linear fitting results.

The linear fitting result obtained in this example ($y = 7.206x + 7.056$) along with the correlation coefficient ($r^2 = 0.9899$) indicate a good fitting effect.

(4) The motor torque sensitivity coefficient obtained from the fitting in step 3 is substituted into the theoretical gravity torque model and compared with the actual driving current curve. At the joint speed commutation, the intercepts at both ends are determined, allowing for the identification of the current values corresponding to the forward and reverse friction forces. Figure **19** illustrates the comparison results of the two curves.

The scheme has been verified on Joint 2, as shown in Figure **16**. It is also applicable to joints with similar dynamic properties, such as Joints 3 and 4, and requires a high degree of smoothness in the current curve.

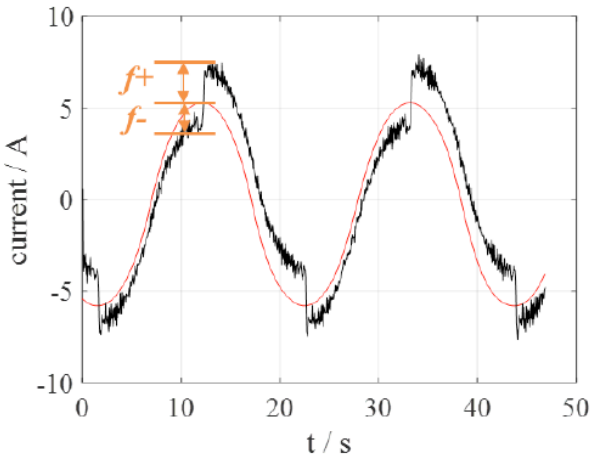

Figure 19: Identification of gravity torque and actual drive current curve.

3.5. Experiment and Analysis of Joints 3–5 and Their Uniaxial Identification

Joints 3 to 5 of this robot experience significant vibrations during movement due to their mechanical structure. Additionally, the underlying driver causes two-phase superposition, resulting in high noise levels in the drive current. Furthermore, since Joints 3 to 5 are positioned at the upper end of the robot, the gravity torque is relatively small, leading to an overall small amplitude of the driving torque, which complicates their identification. Consequently, obtaining an accurate identification model for these joints is challenging, limiting the analysis to qualitative assessments only.

For Joint 3, we maintain the vertical posture of Joint 2 while Joints 4 to 6 are positioned in a straight line. Joint 3 undergoes a reciprocating motion with uniform acceleration and deceleration within a range of ±45°, with four different levels of motion speed set to analyse

the relationship between driving current and speed. Figures **20** to **23** present the resulting curves from the four groups of exercise experiments.

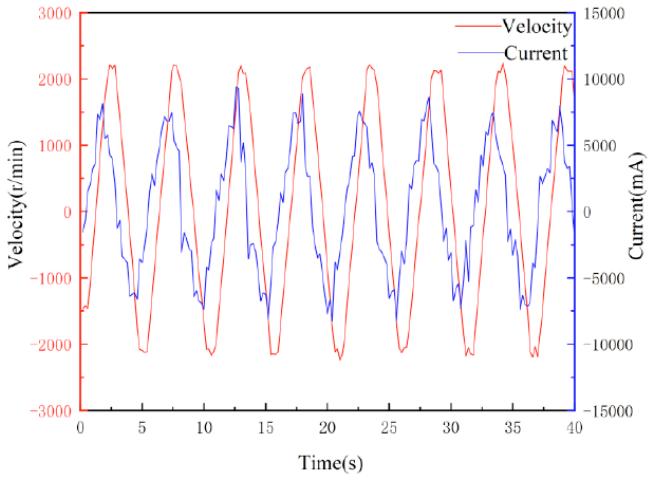

Figure 20: The joint 3 speed and current curve at 2100r/min.

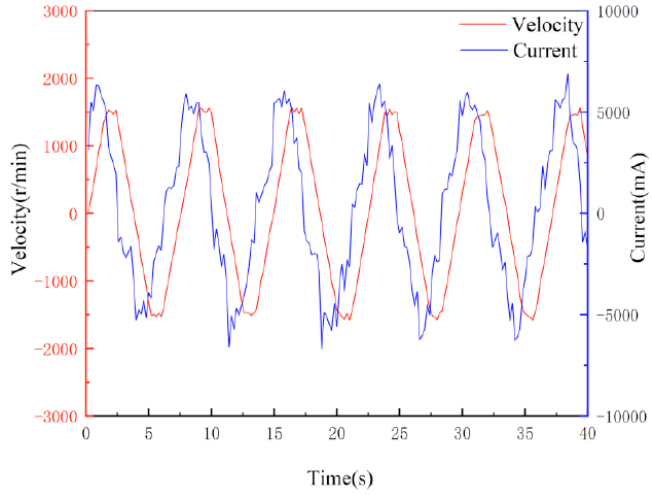

Figure 21: The joint 3 speed and current curve at 1500r/min.

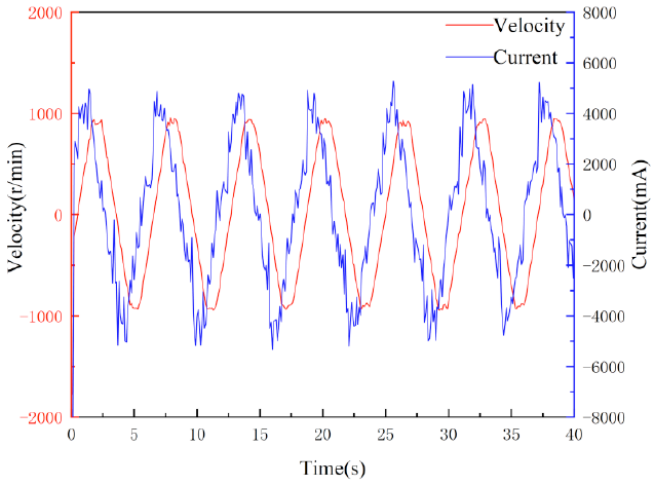

Figure 22: The joint 3 speed and current curve at 950r/min.

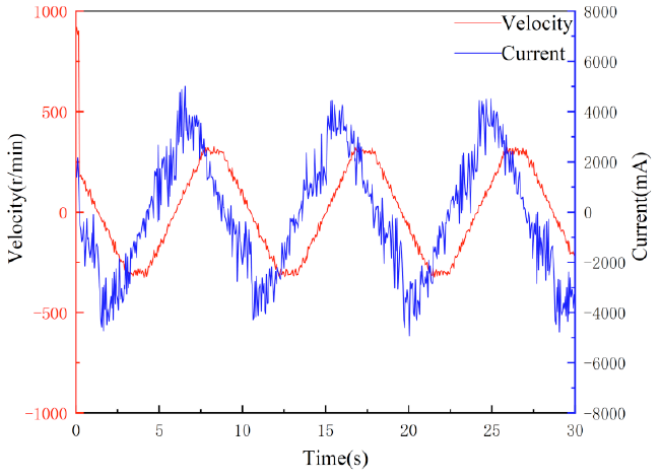

Figure 23: The joint 3 speed and current curve at 300r/min.

The results from the four experimental levels indicate that the peak value of the driving current corresponding to different reciprocating motion cycles fluctuates significantly at higher rotational speeds. Additionally, the curve waveforms become distorted and difficult to identify. Therefore, the last set of experiments is employed for identification. To address the issue of high current noise, the collected current curve is smoothed using a five-point averaging method. While a higher degree of filtering results in a smoother curve, it also carries the risk of losing important details and trends in the waveform; thus, repeated attempts are necessary.

After filtering and eliminating the friction during joint commutation, the resulting driving torque is presented in Figure **24**. As shown, the similarity to a sinusoidal waveform is 0.9744, indicating that fitting can be performed, allowing for subsequent identification.

The identification scheme described in Section 3.4 is applied, and the linear fitting result is displayed in Figure **25**.

The fitting curve is $y = 4.908x + 3.103$, the fitting degree is $r^2 = 0.9804$ and the fitting effect is good. Thus, the torque sensitivity coefficient of joint 3 is 4.9. The currents corresponding to the forward and reverse friction forces of this joint are 1.928 and 1.136 A, respectively.

Hence, the identification dynamic model of joint 3 is obtained, as shown in formula (6) below.

$$I_3 \approx \frac{G_3(\theta)}{4.908} + \begin{cases} 1.928 & v > 0 \\ -1.136 & v < 0 \end{cases} \tag{6}$$

Due to the high noise of the joint 3 drive current, the noise amplitude is equivalent to the friction force value;

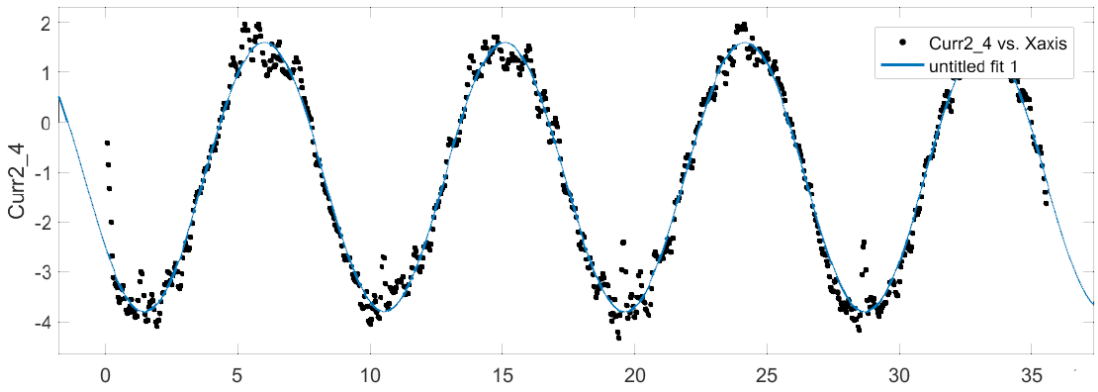

Figure 24: The sine fitting result of the current curve after removing friction.

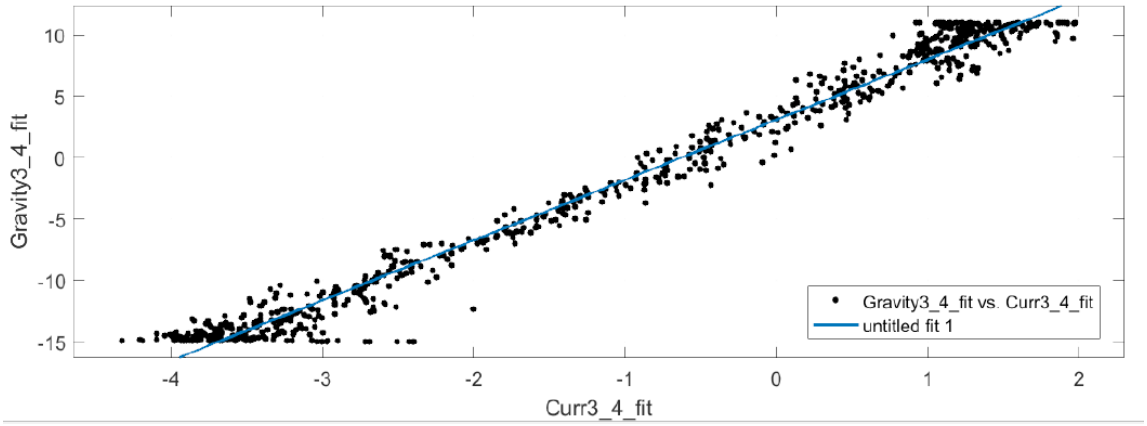

Figure 25: The fitting results of the joint 3 theoretical gravity torque and the friction-less driving current curve.

thus, the method of secondary filtering is adopted. However, secondary filtering has an impact on the accuracy of the identification results. This result is the highest fitting result after several attempts.

For joint 4 of the robot, three motion speeds are set for the reciprocating motion experiment. The obtained joint 4 motion speed and driving current curves are shown in Figures **26**–**28**, respectively.

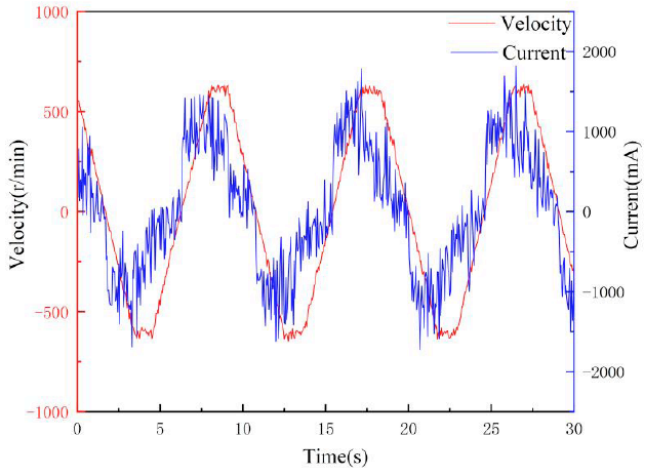

Figure 26: The joint 4 speed and current curve at 20% speed.

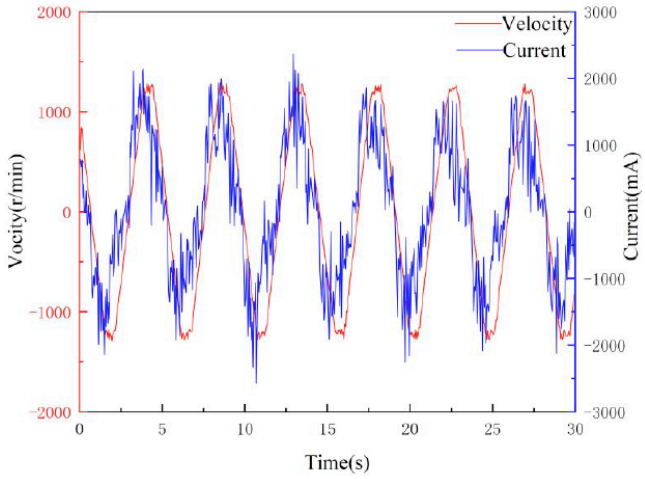

Figure 27: The Joint 4 speed and current curve at 40% speed.

As shown in these figures, the noise in the driving current of Joint 4 is excessively high, comparable to its own driving torque amplitude. Even after secondary filtering, obtaining accurate results remains challenging, with the fitting degree consistently falling below 0.8. This indicates that identification cannot be accomplished with the existing experimental data. However, the friction force of Joint 4 can be

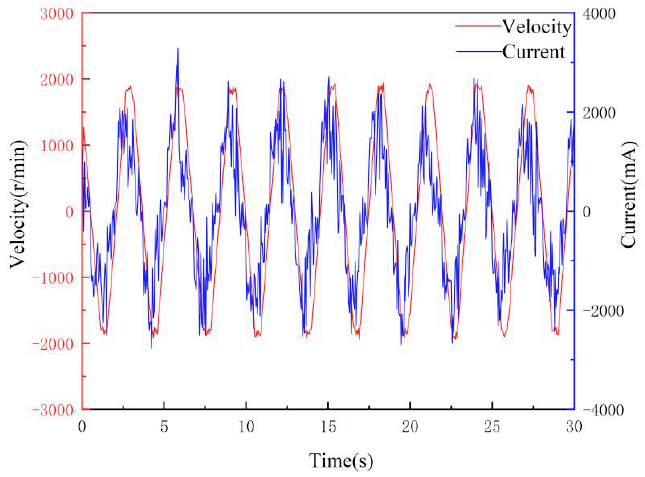

Figure 28: The joint 4 speed and current curve at 60% speed.

qualitatively analyzed by examining the current curve. In Figure **26**, a sudden change in friction force related to the direction of speed is evident. Additionally, when Joint 4 transitions from the uniform motion phase to the deceleration phase, the driving torque experiences a sudden drop, suggesting the presence of a component associated with acceleration direction. Thus, it can be inferred that the driving torque of Joint 4 consists of the basic gravity torque, the forward and reverse frictional forces, the frictional force related to acceleration direction, and possibly a significant inertial force.

For Joint 5, three motion speeds are established for the reciprocating motion experiment. The resulting motion speed and corresponding driving current curves for Joint 5 are displayed in Figures **29** to **31**.

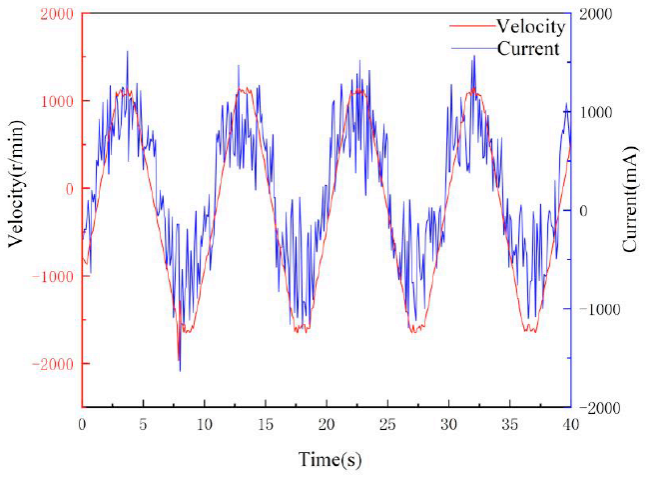

Figure 29: The joint 5 speed and current curve at 20% speed.

As shown in the figures, compared to Joint 4, the driving current of Joint 5 exhibits higher noise levels and is closer to its own driving torque amplitude, making it challenging to obtain accurate identification results. Furthermore, a qualitative analysis of the friction force in Joint 5 reveals a strong correlation between the driving current and movement speed. This characteristic is similar to that of Joint 1, as Joint 5 is located at the end of the mechanism, where the influence of gravity torque on the driving torque is minimal, highlighting its pronounced viscous friction properties.

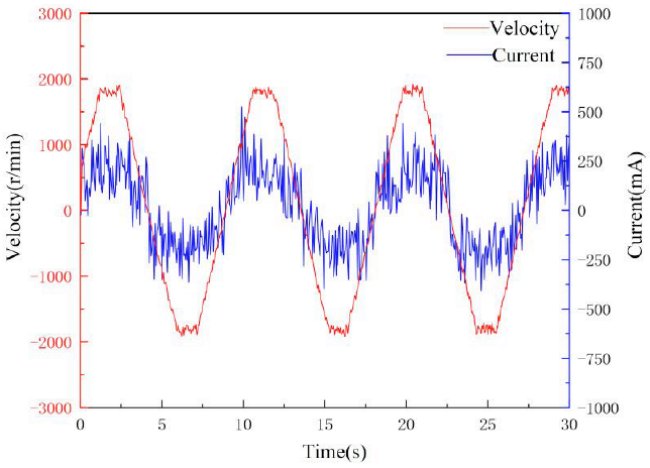

Figure 30: The joint 5 speed and current curve at 40% speed.

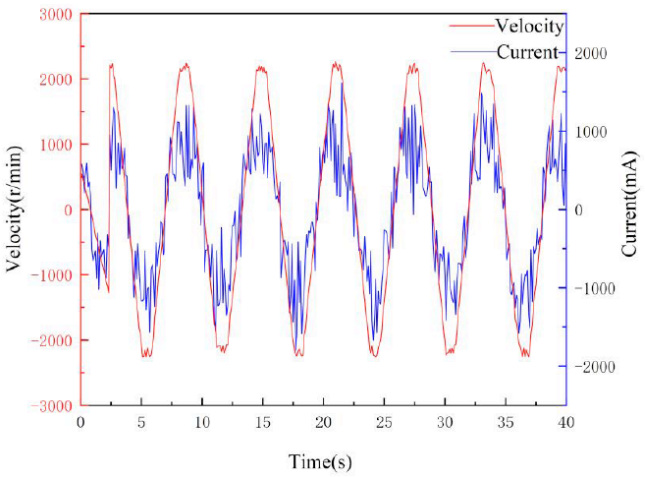

Figure 31: The joint 5 speed and current curve at 60% speed.

3.6. Verification Experiment of Multi-Axis Comprehensive Trajectory Motion

To verify the accuracy of the obtained dynamic model, a multi-axis comprehensive trajectory motion experiment is designed following the identification of the single-axis dynamic model for each joint based on the robot body. The position-time curves for each joint during the experiment are presented in Figure **32**. In this set of experiments, Joints 1 to 5 all executed reciprocating motions with uniform acceleration within their individually set ranges.

The comparison between the predicted driving current of Joints 1 and 2 and the actual collected

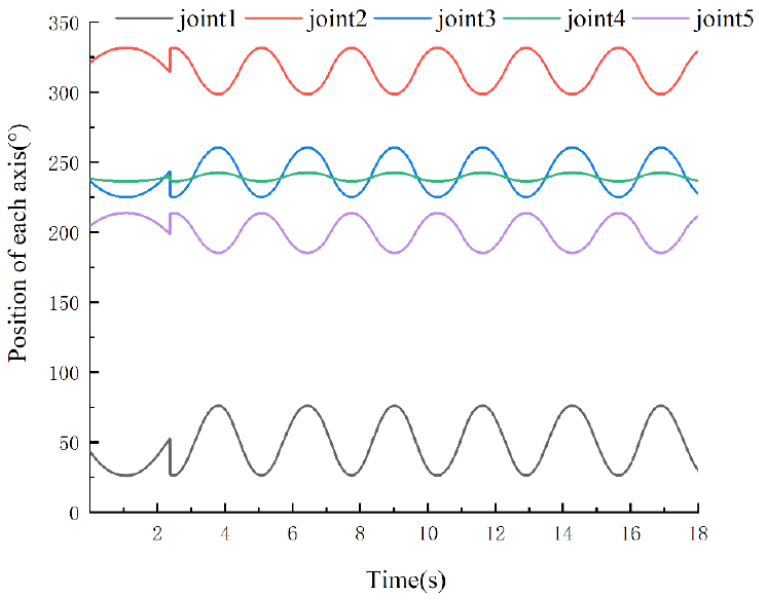

Figure 32: The 5 joints' speed and current curve at 60% speed.

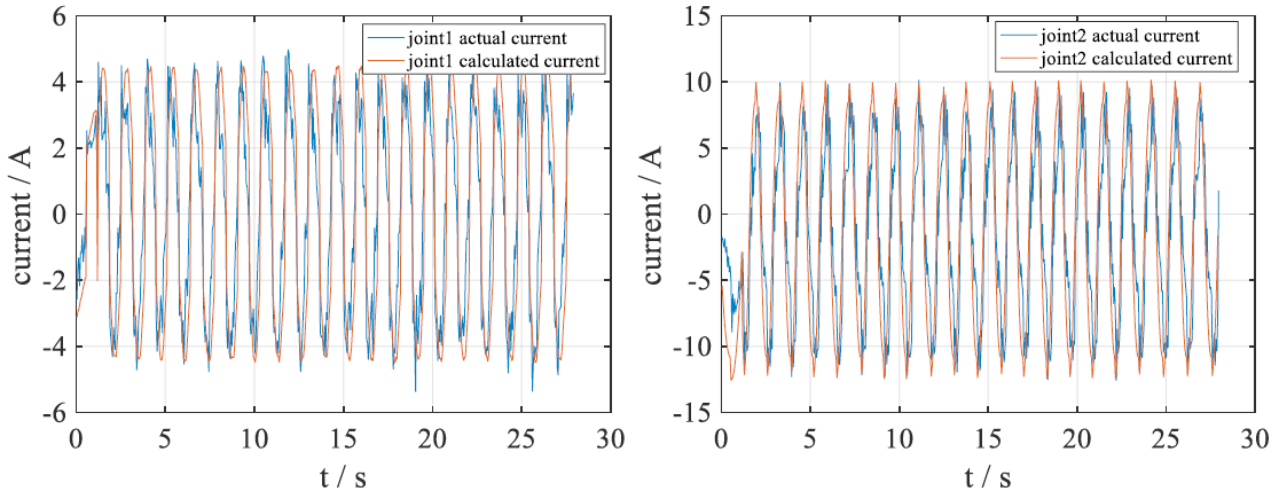

(**a**) joint 1 (**b**) joint 2

Figure 33: Comparison of current prediction of joint 1 and joint 2 and actual results of trajectory motion.

values is shown in Figure **33**. The prediction results are relatively accurate; however, Joints 3 to 5 cannot be predicted at this time due to the inability to obtain an accurate identification model.

4. CONCLUSION

This study introduces a dynamic parameter identification method based on the Lagrangian approach, effectively identifying the dynamic models of joints in a multi-degree-of-freedom manipulator. Our findings indicate that joint posture and operating speed significantly influence driving torque, particularly in joints 1 and 2. This method not only mitigates the impact of joint friction but also determines the motor torque sensitivity coefficient, enhancing control precision. Compared to traditional high-cost sensor methods, this approach offers a more economical solution while emphasizing the importance of theoretical validation. Despite its contributions, limitations remain, particularly in the identification of joints 3 to 5 due to high noise and low gravitational torque. Future research should focus on advanced signal processing techniques, the development of refined dynamic models, and the application of this method across various robotic systems to assess its broader applicability. This work lays a foundation for further advancements in robotic control and smart manufacturing technologies.

CONFLICTS OF INTEREST

No potential conflict of interest was reported by the authors.

REFERENCES

[1] Han Yon. Research on collaborative robot model identification method and human-computer interaction control technology [D]. Shanghai Jiaotong University 2020; 3-5.

[2] Fang Junwei, Wang Binrui, Xie Shenglong, Ren Haijun. Industrial robot dynamics parameter distribution identification and zero-force control teaching [J]. Mechanical Design and Manufacturing. 2021.

[3] Chen Saixuan. Research on zero-force control and collision detection technology of collaborative robots [D]. University of Science and Technology of China 2018; 61-63.

[4] Zhang Tie, Liang Xiaohong, Qin Binbin, Liu Xiaogang. SCARA robot dynamics parameter identification based on Newton's Euler method [J]. Journal of South China University of Technology, 2017; 45(10): 129-130.

[5] Jidong Jia, Minglu Zhang, Changle Li, Chunyao Gao, Xiezhe Zhang, Jie Zhao. Improved dynamic parameter identification method relying on proprioception for manipulators [J]. Nonlinear Dynamics. 2021; 1-16.

[6] Sun Jing, Han xueyan, Li Tong, Li Shihua. Dynamic Parameter Identification of a Pointing Mechanism Considering the Joint Clearance [J]. Robotics 2021; 10(1): 36. https://doi.org/10.3390/robotics10010036

[7] Pan Bingwei, Lv Yan, Jiang Jinfeng, Xue Peijiao. Research on the dynamic parameter identification method of collaborative robots [A]. Shanghai Electric Technology 2019; 12(4): 1-2.

[8] Claudio Urrea, Jose Pascal. Design and validation of a dynamic parameter identification model for industrial manipulator robots [J]. Archive of Applied Mechanics. 2021; 1-27. https://doi.org/10.1007/s00419-020-01865-2

[9] Li Yongquan, Wu Pengtao, Zhang Yang, Zhang Lijie. Dynamic parameter identification and control of spherical two-degree-of-freedom redundant drive parallel robot system [J]. China Mechanical Engineering 2019; 30(16): 1967-1968.

[10] Armstrong. B, Khatib O, Burdick J. The explicit dynamic model and inertial parameters of the PUMA 560 arm [C]. Proceedings of 1986 IEEE International Conference on Robotics and Automation. San Francisco, CA, USA: IEEE, 1986; 510-518. https://doi.org/10.1109/ROBOT.1986.1087644

[11] Chan S P. An efficient algorithm for identification of robot parameters including drive characteristics [J]. Journal of Intelligent and Robotic Systems, 2001; 32(3): 291-305. https://doi.org/10.1023/A:1013918927148

[12] Sousa C. Dynamic model identification of robot manipulators: solving the physical feasibility problem [D]. Coimbra: University of Coimbra, 2014.

[13] Wu Zhiyun, Fu Limin. Finite element algorithm of inertial parameters of robot operator[J]. Journal of Inner Mongolia University of Technology 1995; 14(3): 7-11.

[14] Zhang Shiyuan, Dai Jun, Deng Hua. Dynamic parameter identification of a six-degree-of-freedom robotic arm[A]. Manufacturing Automation 2021; 43(3): 36-37.

[15] Cai Zixing. Robotics [A]. Beijing: Tsinghua University Press, 2009; 73-75.

[16] Arun Banerjee. Flexible Multibody Dynamics: Algorithms Based on Kane's Method [B]. CRC press.2022. https://doi.org/10.1201/9781003231523

[17] Saixuan Chen, Jie Yang1, Guohua Cui, Fuzhou Niu, Baiqiang Yao and Yu Zhang. Robot Zero-Moment Control Algorithm Based on Parameter Identification of Low-Speed Dynamic Balance [J]. Computer Modeling in Engineering & Sciences 2023; 134(3): 2021-2038. https://doi.org/10.32604/cmes.2022.022669

Received on 04-10-2024 Accepted on 11-11-2024 Published on 23-11-2024

https://doi.org/10.31875/2409-9694.2024.11.09